Isotopic tracers of sources of water for springs from the Edwards Aquifer, Central Texas, USA

Lijun Tian, Yongli Gao, Guang Yang, Benjamin Schwartz, Binggui Cai, Christopher Ray, Yunxia Li and Haibin Wu

ABSTRACT

The Edwards Aquifer (EA) in Central Texas provides water supply for over two million people and contains springs that are hydrologically and ecologically important to the region. The residence time of groundwater in the EA ranges from a few days to many thousands of years, since water in the aquifer is contained and transported within both matrix porosity and large conduits. In this study, stable isotopes of water from five springs are investigated for tracing the origin of water and hydrological processes in the EA system during 2017–2019. There is a quick response of the isotopic signals measured at these springs to changes in the isotopic compositions of precipitation. By utilizing an isotope mixing model, we have identified sources of water for these springs with a bi-modal distribution of groundwater supply in the EA: water supplied from deep groundwater with a longer residence time (an average of 67%) and supplemental epikarst interflow with a shorter residence time (an average of 33%). The evolution of hydrochemical water types from HCO_3–Ca to HCO_3·Cl–Ca·Mg along the EA flowpaths indicates that inputs from epikarst interflow are greater in springs within the artesian zone than the springs within the contributing zone.

Key words | Central Texas, Edwards Aquifer, hydrochemistry, isotope mixing model, karst springs, stable isotopes

HIGHLIGHTS

- Stable isotope tracers were utilized to understand the origins of spring water and hydrological processes in the Edwards Aquifer.
- There is a quick response for isotopic signals in spring water to changes in the isotopic compositions of precipitation.
- There is elevated input from epikarst interflow for spring water balance in the artesian zone than the contributing zone.

Lijun Tian (corresponding author)
Haibin Wu
Key Laboratory of Cenozoic Geology and Environment,
Institute of Geology and Geophysics, Chinese Academy of Sciences,
Beijing, China
E-mail: *tianlijun@mail.iggcas.ac.cn*

Lijun Tian
Yongli Gao
Guang Yang
Christopher Ray
Yunxia Li
Department of Geological Sciences,
University of Texas at San Antonio,
San Antonio, TX, USA

Guang Yang
College of Water and Architectural Engineering,
Shihezi University,
Shihezi, China

Benjamin Schwartz
Edwards Aquifer Research and Data Center,
Texas State University,
San Marcos, TX, USA

Binggui Cai
School of Geographical Sciences,
Fujian Normal University,
Fuzhou, China

Yunxia Li
College of Resources and Environmental Sciences,
Hunan Normal University,
Changsha, China

Haibin Wu
Center for Excellence in Life and Paleoenvironment,
Chinese Academy of Sciences,
Beijing, China
and
College of Earth and Planetary Sciences,
University of Chinese Academy of Sciences,
Beijing, China

doi: 10.2166/nh.2021.011

INTRODUCTION

The Edwards Aquifer (EA), located along the southeastern edge of the Edwards Plateau in Texas, is one of the most prolific artesian aquifers in the world (Sharp & Banner 1997). The EA is the major source of potable water for two million people and the primary water supply for agricultural and industrial use in Central Texas (Schindel *et al.* 2004). The EA is primarily recharged by surface runoff that feeds the numerous streams and creeks originating in the Texas Hill Country. The primary natural discharge points from the EA are springs in the artesian zone, especially those along the Balcones Fault Zone (Hunt *et al.* 2019). These springs have supported natural ecosystems, human populations, and urban development in Central Texas for thousands of years. However, water shortages can occur in the EA due to excessive pumping of groundwater and periodic droughts (Tian *et al.* 2020).

The EA confined/artesian zone contains highly variable (in time and location) mixtures of waters with residence times ranging from a few days to many thousands of years (Eberts *et al.* 2011). Radiocarbon dating is not a reliable groundwater dating method in karst aquifers (Maloszewski & Zuber 1991) because the contribution of 'dead' carbon from the dissolution of calcite/dolomite would lead to a significant over-estimation of the groundwater's age. Hunt *et al.* (2016) determined apparent ages for well water from the EA by applying a $^{3}H/^{3}He$ dating method, which indicated that the groundwater is the result of mixing of both modern (less than 60 years) and premodern (higher than 60 years). Kuniansky *et al.* (2001) utilized the finite-element method to model travel times for water within the aquifer and estimated a range of 350–4,300 years, assuming a flowpath from the West Nueces River Basin to Comal Springs. Dye tests in the EA usually reveal high velocities and short residence times. For example, Hunt *et al.* (2005) utilized fluorescein dye to determine that the water arrived at Barton Springs between 7 and 8 days from the recharge cave.

The rocks hosting the EA contain large voids such as conduits, caves, fractures, and fissures, as well as matrix porosity (Hovorka *et al.* 1995; Chen *et al.* 2012), which facilitate recharge of the aquifer due to precipitation. Hydrographs from wells and/or springs can be used to analyze the structure and response of the hydrogeological system (Halihan & Wicks 1998). However, the range of mechanisms affecting hydrographic responses has not been thoroughly investigated in the EA region (Zhang *et al.* 2020). Hydrochemical and isotopic analysis of spring water in a watershed are particularly suitable for tracing the origin of water and providing information on hydrological processes (e.g. Araguás-Araguás *et al.* 2000; Marfia *et al.* 2004; Martinez *et al.* 2015; Shakya *et al.* 2019). This research has investigated isotopic signatures of five springs from the EA region through monthly sampling during 2017–2019. Changes in the isotopic compositions of the springs were compared with the isotopic signatures in local precipitation. The objectives of this study were: (1) to document the spatial and temporal variations in the isotopic composition of spring water and precipitation, (2) to investigate the isotopic response of spring water to the isotopic variations in precipitation, and (3) to determine the water mass balance for different sources potentially feeding springflow.

STUDY AREA

Hydrogeologic setting

The EA is an extensively karstified groundwater flow system developed in limestone rocks deposited during the Cretaceous (Schindel 2019). As shown in Figure 1, the EA system has been geographically divided into three major hydrogeologic zones: the contributing zone (or drainage area), the recharge zone, and the artesian zone (Stone & Schindel 2002). The contributing zone collects rainwater and springflow, which forms the headwater of major streams in the region; then the surface runoff is conveyed into the recharge zone without significant loss. The recharge zone approximately overlies the Balcones fault zone, allowing for vertical downward movement of surface water into the EA. The artesian zone, where the EA is confined, contains most of the large production wells that pump water out of the EA. The general flowpaths of water within the EA are from

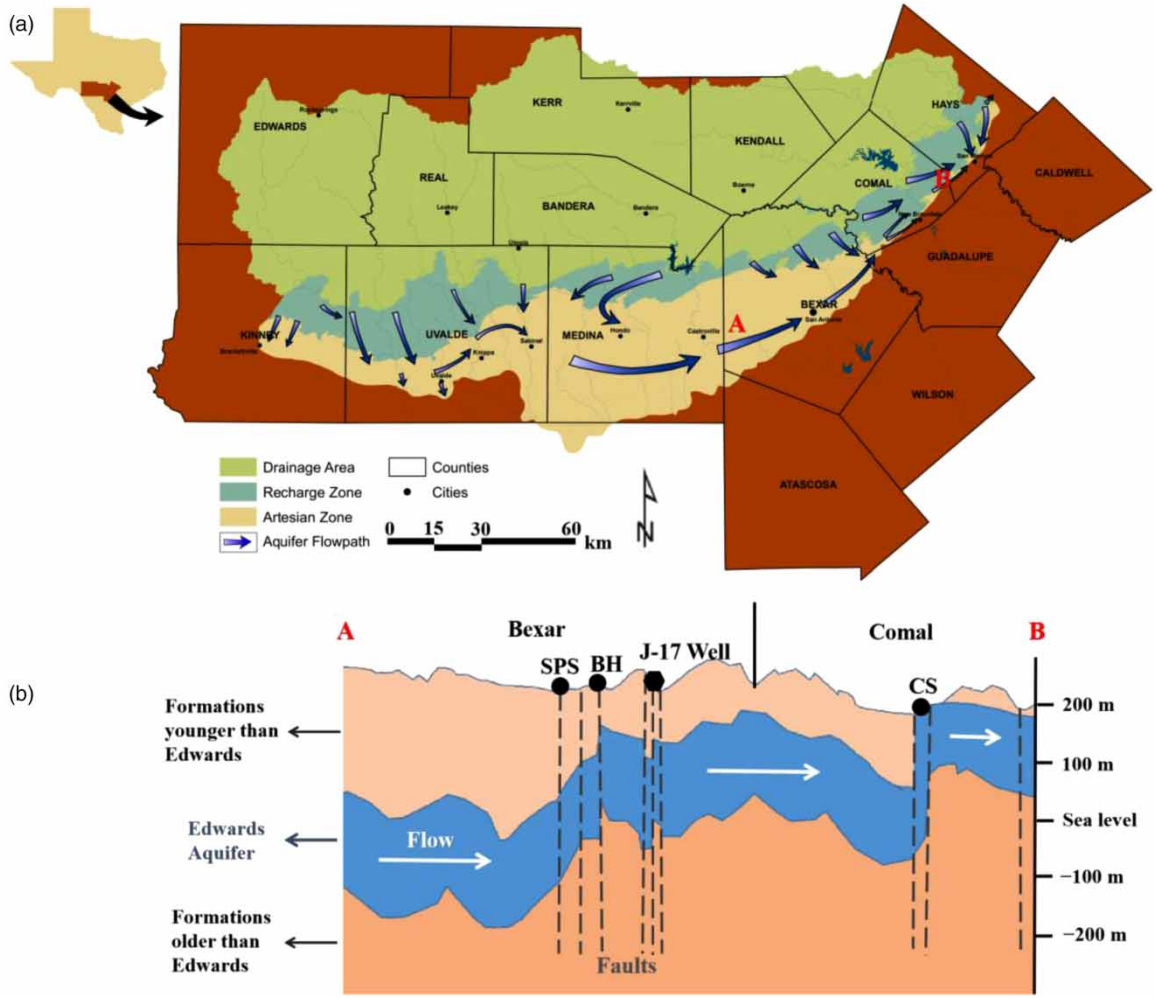

Figure 1 | General flowpaths of water within the EA (a) and the hydrogeologic cross section along the flowpath from points A to B (b). The locations of three springs and the J-17 Well within the artesian zone are indicated. The base map is available from the Edward Aquifer Authority (https://www.edwardsaquifer.org/science-maps). The hydrogeologic cross section within Bexar and Comal Counties is adapted from Klemt *et al.* (1979).

the north to the south in the contributing zone, then from the southwest to northeast in the artesian zone (Figure 1(a)).

The hydrogeologic cross section within Bexar and Comal Counties is shown in Figure 1(b). The Blue Hole (BH) is the largest spring of 'The San Antonio Springs', which is located at a nature preserve called the Headwater Sanctuary on the campus of the University of Incarnate Word. The San Pedro Springs (SPS) is located a few miles northwest of downtown San Antonio, directly adjacent to the campus of San Antonio College. The Comal Spring (CS) is the largest spring in Texas, and it is located at the base of a steep limestone bluff in Landa Park of New Braunfels. The altitudes for BH, SPS, and CS are 206, 202, and 192 m, respectively. The J-17 Index Well is located at Fort Sam Houston in San Antonio. The J-17 Well is on a major flowpath in the EA and responds quickly to pumpage and recharge. Thus, the water level variation of J-17 Well is a general indicator of the amount of water within the EA. Springflow at CS becomes intermittent when the water level measured at J-17 Well drops below 192 m; flow at BH ceases when the J-17 Well level is below 207 m; and flow at SPS ceases when the J-17 Well level is below 201 m. No flow was recorded at BH and SPS several times during our sampling interval. Water was constantly issuing from CS during our sampling interval; however, historically, flow ceased during the 1950s drought when the J-17 Well dropped to 187 m (Cox *et al.* 2009).

Climatic and weather conditions

The research area, located in Central Texas, has a transitional humid subtropical climate, with hot summers and generally mild winters with infrequent severe freezes. The climatic parameters (temperature and precipitation amount) at the City of Boerne during 2017–2019, together with those from 1981 to 2010 for comparison, are summarized in Figure 2. The weather station site is within 20 km from our precipitation sampling site, and the precipitation falling on the contributing zone should be the source of water for the springs in the artesian zone.

There were high summer temperatures and increasing seasonal variabilities of precipitation during 2017–2019, compared with long-term averages in the period 1981–2010 (Figure 2). Monthly precipitation amounts varied between 53 mm (January) and 118 mm (May) derived from the long-term (1981–2010) monthly means, and the monthly temperature varied between 9.0 °C (January) and 27.6 °C (August). Notably, the precipitation amounts in the summer seasons (June–August) were significantly lower than the corresponding averages. However, September 2018 was the wettest September on record in Boerne: 360 mm in September 2018 compared with an average of 88 mm during 1981–2010. The average annual precipitation amount was 964 mm during 1981–2010. Annual precipitation amounts for 2017 (733 mm) and 2019 (672 mm) were lower than the average, whereas the annual precipitation amount for 2018 (1,092 mm) was higher than the average. The annual mean temperatures during 2017–2019 were 20.3, 19.4, and 19.3 °C respectively, which were higher than an average of 18.8 °C from 1981 to 2010.

Groundwater hydrographs

The water levels of the J-17 Well, discharge of CS, along with meteorological data during 2017–2019 are shown in Figure 3. The springflow of CS originates from groundwater flow in the southwest (Figure 1), and the flowpath moves past the J-17 Well on its way toward CS. The underground flow might take a few years based on MODFLOW calculations for the deep groundwater with a long residence time. However, the hydrograph illustrates both J-17 Well levels and CS springflows quickly respond to net precipitation (precipitation–evaporation), and there is almost no lag between CS springflow and J-17 Well levels (Figure 3). The fast response to net precipitation for both sites should be due to additional inputs from surface runoff or epikarst interflow. Our spring water are collected at the spring orifices to avoid inputs from surface runoff or stormwater. There are typical karst features of fissure, fracture, sinkholes, and caves near the spring sites, which facilitate surface water infiltration. Therefore, we conclude that the additional supplement for the spring water balance is epikarst interflow or shallow groundwater with short residence time.

METHODS

Water sampling and field measurements

This research has investigated isotopic signatures of five springs from the EA, two springs (BS1 and BS2) from the unconfined section and three springs (BH, SPS, and CS)

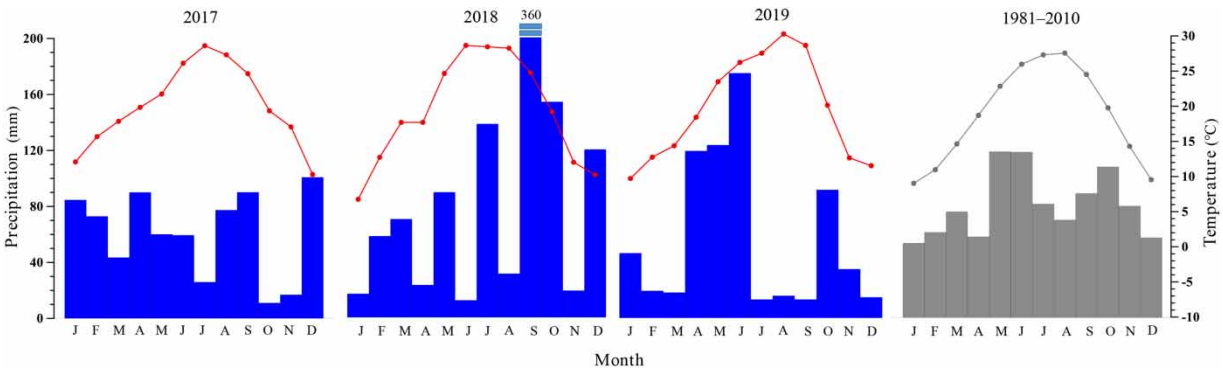

Figure 2 | Monthly air temperature and precipitation amount in the City of Boerne during 2017–2019, and their long-term average values during 1981–2010. The meteorological data are available from the National Climatic Data Center archives (http://www.ncdc.noaa.gov).

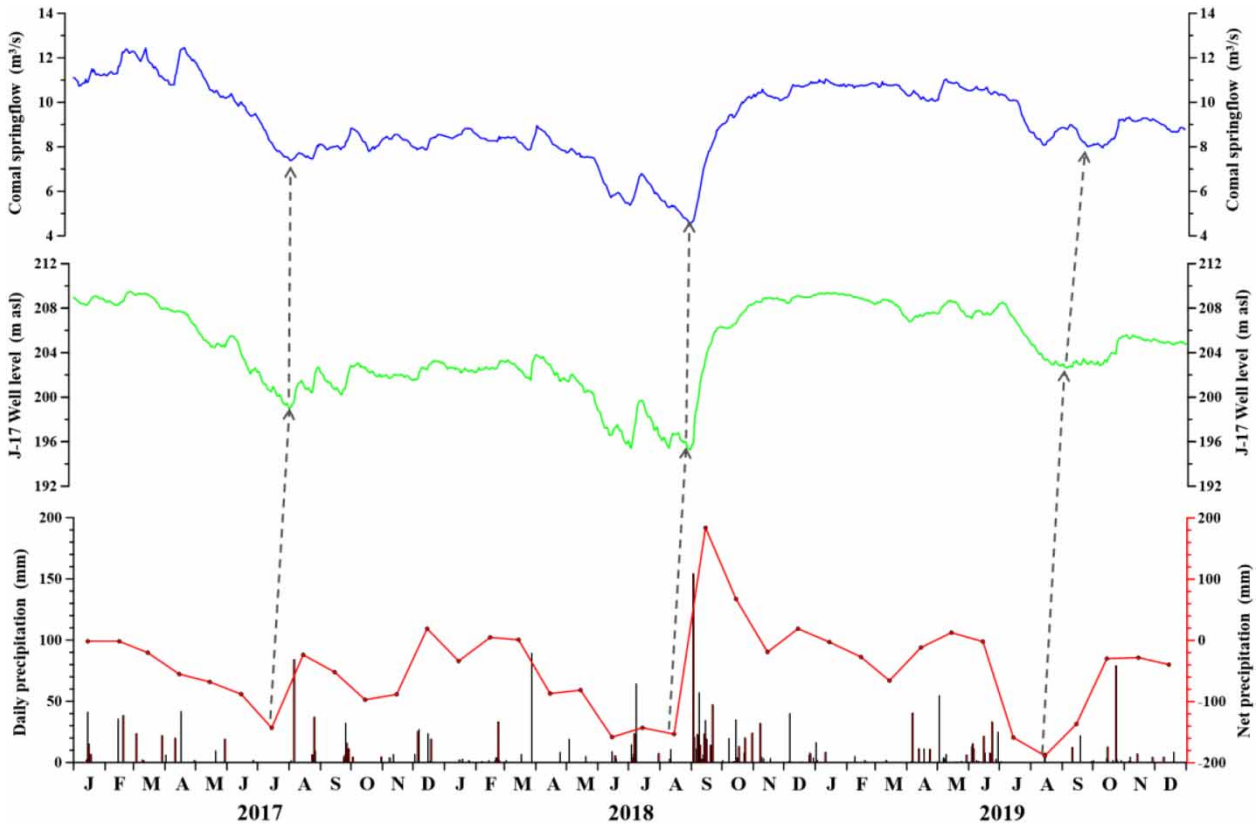

Figure 3 | Responses of CS discharge and J-17 Well level to precipitation during 2017–2019. The dashed lines indicate the base flow conditions. The daily precipitation data at the City of Boerne are available at http://www.ncdc.noaa.gov. The net precipitation data of Central Texas was calculated based on the monthly precipitation and evaporation data at https://waterdata.usgs.gov. The J-17 Well level data is available at https://www.waterdatafortexas.org. The springflow of CS is available at https://txpub.usgs.gov/projects/spring_calc/.

from the confined section, by monthly sampling during 2017–2019, along with the isotopic signatures in precipitation. Locations, altitudes, and site descriptions of the five investigated springs are listed in Supplementary Material, Table S1. Springs termed BS1 and BS2 emerge from the contributing zone and represent the headwater of the Upper Cibolo Creek (UCC) watershed. The UCC generally flows in a southerly or easterly direction across the UCC watershed. Two major springs, BH and SPS, discharge from the artesian zone proximal to the downtown region of San Antonio. CS lies within the transition of the recharge zone/artesian zone. Precipitation samples were collected after each rain event in an open area near the main campus of UTSA (29°35′N, 98°38′W). Locations and photos for these sampling sites are shown in Figure 4 and Supplementary Material, Figure S1, respectively.

A total of 148 spring samples were collected during 2017–2019: 36 samples for both BS1 and BS2, 32 samples for CS, 29 samples for SPS, and 15 samples for BH. All investigated springs were sampled monthly in general; however, spring discharge of BH and SPS had ceased many times during our sampling interval.

Samples collected for stable isotope, cation, and anion analysis were filtered using 0.2-μm filters at the time of collection and stored in sterilized HDPE bottles. The bottles and caps were rinsed three times with filtered water, sealed with parafilm, and refrigerated until the time of analysis.

Water temperature, electrical conductivity (EC), total dissolved solids (TDS), and pH were measured at the time of collection. Water temperature, EC, and TDS were measured with a YSI® 556 MPS handheld multi-parameter sensor, while pH was measured with a Hach® sensION1 handheld pH meter. EC and pH sensors were calibrated before each sampling field.

Daily rainwater was collected in a 10-cm diameter high capacity Stratus® rain gauge. A ping-pong ball was placed at

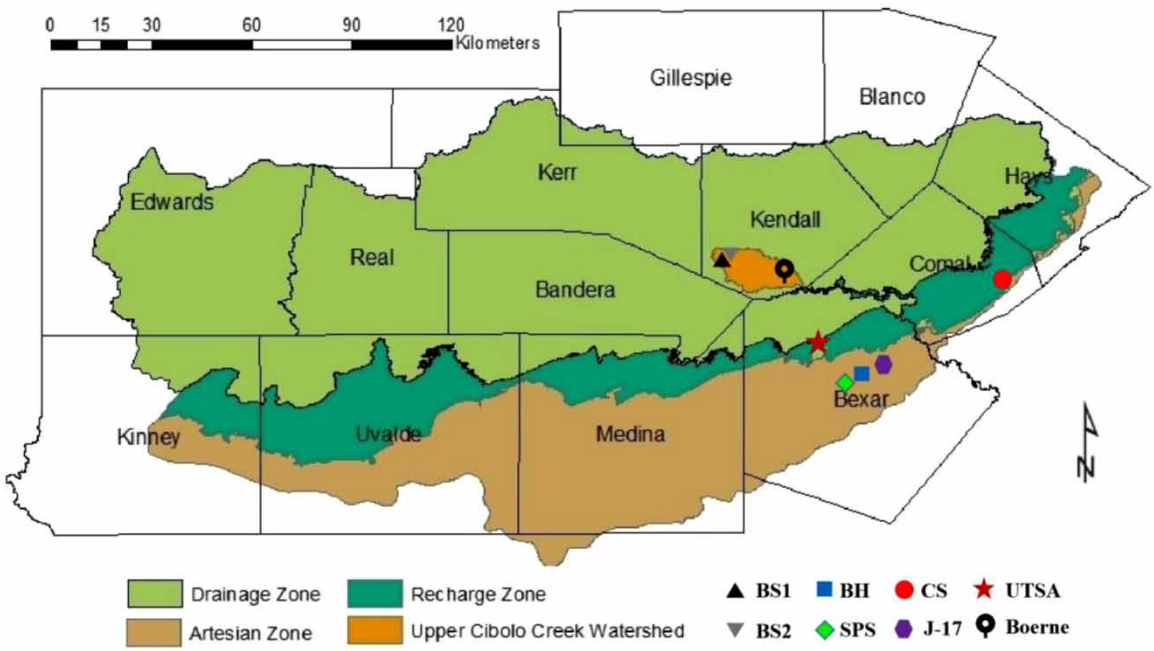

Figure 4 | Locations of the sampling sites and J-17 Well in the EA region.

the mouth of the rain gauge to prevent evaporation (Michelsen *et al.* 2018). Sample collection was usually performed during the morning at about 8 a.m. when rain events happened at nights or early mornings, while some collections were performed at other times when the rainfall occurred during the daytime. The rain gauge was emptied and cleaned after each rain event, and sub-samples of the homogenized precipitation were sealed in pre-cleaned bottles, with no headspace, for future $\delta^{18}O$ and δD analysis (Gröning *et al.* 2012).

Laboratory measurements

The concentrations of cations (Ca^{2+}, Mg^{2+}, Na^{+}, K^{+}, and Sr^{2+}) and anions (SO_4^{2-}, Cl^{-}, F^{-}, Br^{-}, and NO_3^{-}) were measured using Dionex ion chromatography (IC) at Texas State University. Water samples with conductivities higher than 0.90 mS/cm were diluted with Milli-Q ultrapure water in a specific ratio before analysis. Milli-Q blanks and standards with dilutions bracketing the range of ion concentrations in the samples were run at the time of analysis.

The alkalinity of filtered water samples was measured by titration with 0.01 mol L^{-1} hydrochloric acid. The pH of our collected groundwater samples generally ranges between 6 and 9, which implies the CO_3^{2-} concentration is negligible, and the alkalinity should be approximately the same as HCO_3^{-} concentration. Thus, we only tested the bicarbonate alkalinity, i.e. HCO_3^{-} concentration, using the bromocresol green-methyl red mixed indicator.

$\delta^{18}O$ and δD measurements for precipitation and spring water samples were performed on a Picarro L2130-i water isotope analyzer (cavity ring-down spectroscopy, CRDS) at the Department of Geological Sciences, University of Texas at San Antonio. Results are reported with δ notation in per mil (‰) relative to the standard Vienna Standard Mean Ocean Water (VSMOW; Craig 1961). The measurement precisions for $\delta^{18}O$ and δD were 0.1‰ (1σ) and 0.4‰ (1σ), respectively. $\delta^{18}O$ and δD are given in the following equations:

$$\delta^{18}O = \frac{[(^{18}O/^{16}O)_{Sample} - (^{18}O/^{16}O)_{VSMOW}]}{(^{18}O/^{16}O)_{VSMOW}} \times 10^3 \text{‰} \quad (1)$$

$$\delta D = \frac{[(D/H)_{Sample} - (D/H)_{VSMOW}]}{(D/H)_{VSMOW}} \times 10^3 \text{‰} \quad (2)$$

Deuterium excess (D-excess), a second-order parameter that combines both oxygen and hydrogen isotopic species, is

defined by the following expression (Dansgaard 1964):

$$\mathrm{D-excess} = \delta\mathrm{D} - 8 \times \delta^{18}\mathrm{O}\ ‰ \tag{3}$$

To investigate the monthly isotopic variability in precipitation, the amount weighted mean isotopic values in precipitation were calculated for monthly intervals corresponding to spring water collection dates during 2017–2019 using the following equation:

$$\delta_{\mathrm{month}} = \frac{\Sigma(P_i\delta_i)}{\Sigma P_i} \tag{4}$$

where P_i refers to the daily precipitation amount, δ_i refers to δD or $\delta^{18}O$ values of daily precipitation, and δ_{month} represents δD or $\delta^{18}O$ values of monthly precipitation.

Isotope mixing model

Based on the analysis of groundwater hydrographs (Figure 3), we speculated that there are both shallow and deep groundwater contributions in the spring discharge mass balance (Hare *et al.* 2021). In the EA context, the shallow groundwater has shorter residence time which could range from days to months for 'quick' response; the deep groundwater has longer residence time which could range from years to centuries for 'slow' response (Hunt *et al.* 2016).

A mixing model based on the principle of isotope mass conservation was established to calculate the contribution rate of different water sources to the compositions of the five springs. We determine the contributions from shallow and deep groundwater for the monthly spring discharge by utilizing the isotope mixing model (one-tracer for two-component). Mass balance calculations for the monthly spring water in the EA are calculated as follows:

$$\delta^{18}\mathrm{O}_{\mathrm{SW}}^{N} = \delta^{18}\mathrm{O}_{\mathrm{DG}}F_{\mathrm{DG}}^{N} + \delta^{18}\mathrm{O}_{\mathrm{SG}}^{N}F_{\mathrm{SG}}^{N} \tag{5}$$

$$1 = F_{\mathrm{DG}}^{N} + F_{\mathrm{SG}}^{N} \tag{6}$$

where ${F_{\mathrm{DG}}}^{N}$ and ${F_{\mathrm{SG}}}^{N}$ are unknown fractions of 'deep groundwater' and 'shallow groundwater' in the month N, respectively. $\delta^{18}O_{DG}$ is the constant oxygen isotope value from the 'deep groundwater' during base flow conditions. ${\delta^{18}\mathrm{O}_{\mathrm{SW}}}^{N}$ and ${\delta^{18}\mathrm{O}_{\mathrm{SG}}}^{N}$ are $\delta^{18}O$ values for 'spring water' and 'shallow groundwater' in the month N, respectively. The $\delta^{18}O$ endmembers are assigned later for water balance calculations.

RESULTS AND DISCUSSION

Hydrochemical data visualization

The field measurements, major ion concentrations, and isotopic analysis for all samples of five investigated springs during 2017–2019 are listed in Supplementary Material, Table S2. The summary statistics of hydrochemical and isotopic parameters of the five springs are listed in Table 1, for each spring is listed separately in Supplementary Material, Table S3. We utilized major cations and major anions to calculate the charge balance error (CBE), and the CBE is mostly clustered within ±5%, with many outside of ±5% and a few outside of ±10%. Thus, the hydrochemical dataset is acceptable for general hydrochemical characterization.

The temperature and pH are consistent among the five springs, with the lowest coefficient of variation (CV), indicating that the major source of the spring water is from the deep underground aquifer. Among water isotopes,

Table 1 | Summary statistics of hydrochemical and isotopic parameters for all samples of five investigated springs during 2017–2019

Parameters	Min	Max	Mean	SD	CV (%)
T (°C)	11.8	25.8	21.6	2.5	11.6
EC (μs/cm)	343.0	1135.0	538.7	99.6	18.5
TDS (ppm)	223.0	738.0	350.1	64.8	18.5
pH	6.2	8.7	7.8	0.5	6.2
$\delta^{18}O$ (‰)	−5.1	−1.6	−4.2	0.6	15.3
δD (‰)	−29.1	−14.4	−23.2	2.6	11.3
D-excess (‰)	−1.7	14.0	10.1	2.9	29.2
Ca^{2+} (ppm)	28.6	100.4	66.1	18.3	27.6
Mg^{2+} (ppm)	0.0	17.4	12.3	5.2	42.0
Na^{+} (ppm)	3.2	28.5	8.8	3.3	37.6
K^{+} (ppm)	0.0	16.4	1.4	2.0	141.5
SO_4^{2-} (ppm)	0.0	49.8	16.3	9.8	60.4
Cl^{-} (ppm)	1.7	39.5	13.7	5.5	40.4
NO_3^{-} (ppm)	1.0	20.1	5.9	2.9	48.6
HCO_3^{-} (ppm)	92.0	322.0	195.7	64.4	32.9

D-excess (29%) is more variable than $\delta^{18}O$ (15%) and δD (11%). The range of concentrations for Ca^{2+} and HCO_3^- are relatively small, with relatively low CVs for Ca^{2+} (28%) and HCO_3^- (33%). The concentration of these ions results from the dissolution of limestone within the EA (e.g. Engesgaard & Christensen 1988; Tian *et al.* 2020), and the spring water are likely supersaturated generally with carbonate in the study area. The concentrations for K^+ and NO_3^- display substantial variabilities among the spring sites, with relatively high CVs for K^+ (142%) and NO_3^- (49%). None of these ions is from the dissolution of limestone in the research area but is more likely associated with human activities (e.g. Jiang *et al.* 2008; Wang *et al.* 2018). Their highly variable concentrations indicate the sources of water not only come from deep groundwater, but with additional supplementary inputs from precipitation, surface runoff, or epikarst interflow.

The correlation coefficients of chemical parameters for the spring samples are shown in Figure 5. There are significant correlations among ion concentrations of NO_3^-, Cl^-, SO_4^{2-}, Mg^{2+}, K^+, and Na^+. Ion concentrations of Mg^{2+} and SO_4^{2-} likely originated from the dissolution of gypsum, while the other ions are related to human activities. Previous studies have indicated elevated chlorine and nitrate levels for surface water and groundwater in the research area (e.g. Morrall *et al.* 2004; Sullivan & Gao 2016). A SWAT model coupled with groundwater flow and contaminant transport models indicated that anthropogenic inputs as well as biogenic

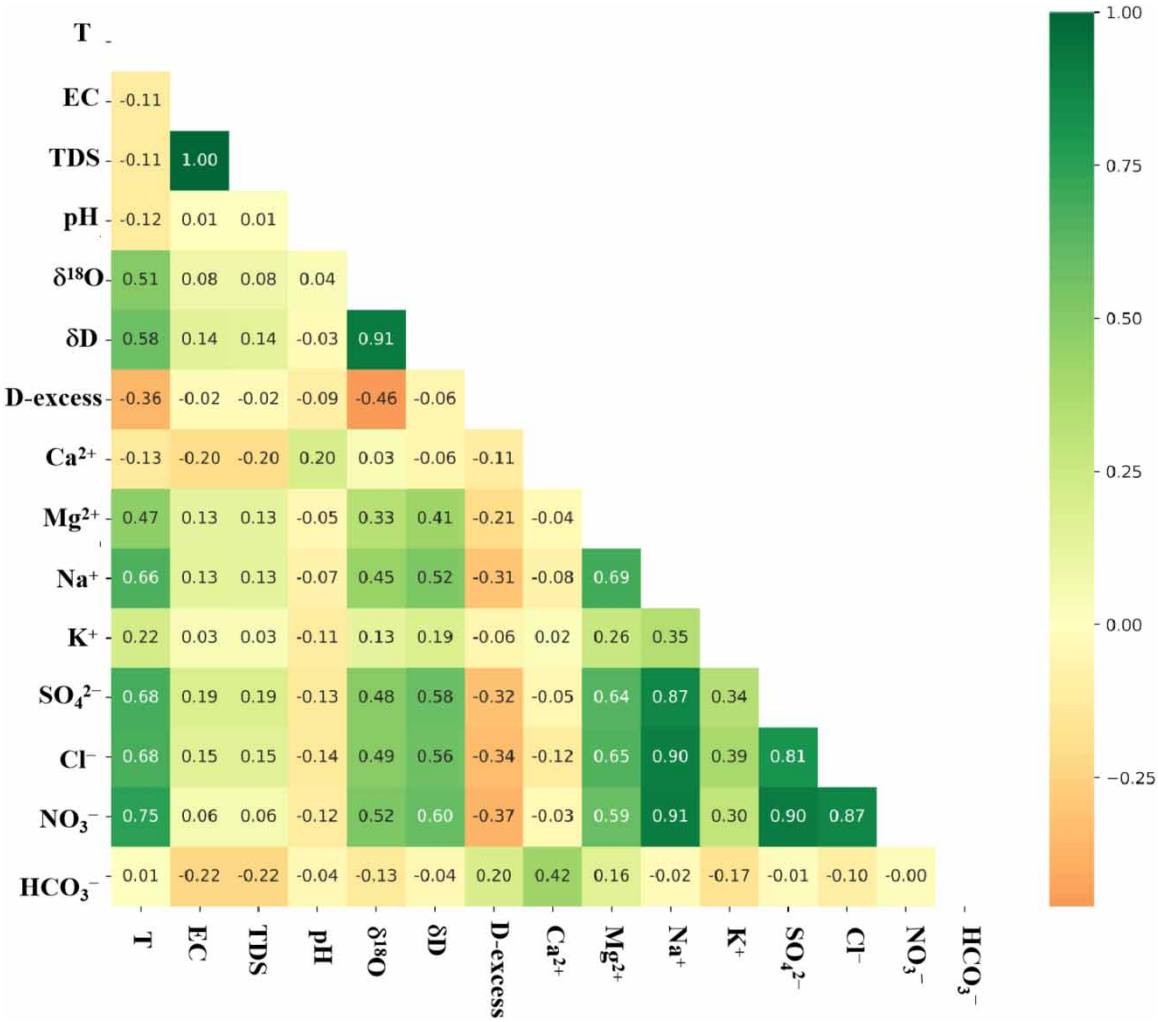

Figure 5 | Correlation coefficients of chemical parameters for the spring samples.

wastes were important sources of nitrate to the EA system (Sullivan *et al.* 2019). D-excess is negatively correlated with $\delta^{18}O$ and δD. The isotopic variations are well correlated with ion concentrations of NO_3^- and Cl^-. The possible reason is that both the isotopic signatures and contaminants of these springs are precipitation input signals. The higher NO_3^- and Cl^- concentrations are not directly from precipitation inputs, but the load of anthropogenic contaminants during the precipitation infiltration.

A Piper diagram displaying relative concentrations of cations and anions for the five springs is shown in Figure 6, and Piper diagrams for each spring are shown separately in Supplementary Figure S2. The relative concentrations of anions and cations for these spring samples are shown in the Schoeller diagram (Supplementary Material, Figure S3). The dominant species in the spring water are Ca^{2+} and HCO_3^- for all five springs, which indicates that the major contribution of ions originates from water–rock interaction within the aquifer. Thus, the water source of these springs is mainly from 'older' deep groundwater. However, occasionally there are elevated concentrations of Cl^-, which may indicate additional supplementary inputs from 'young' water, more directly tied to epikarst interflow or shallow groundwater (Moore *et al.* 2009; Chaudhuri & Ale 2014; Retike *et al.* 2016). There are higher Cl^- concentrations in the three springs (BH, SPS, and CS) from the confined zone than the two springs (BS1 and BS2) from the unconfined zone. The hydrochemical classification also evolves from HCO_3–Ca type to HCO_3·Cl–Ca·Mg type from the contributing zone to the artesian zone, which indicates the springs in the artesian zone might have high contributions of precipitation input.

Isotopic spatiotemporal variations

The cross plots of $\delta^{18}O$ and δD for the spring water and precipitation are provided in Figure 7; the cross plot only

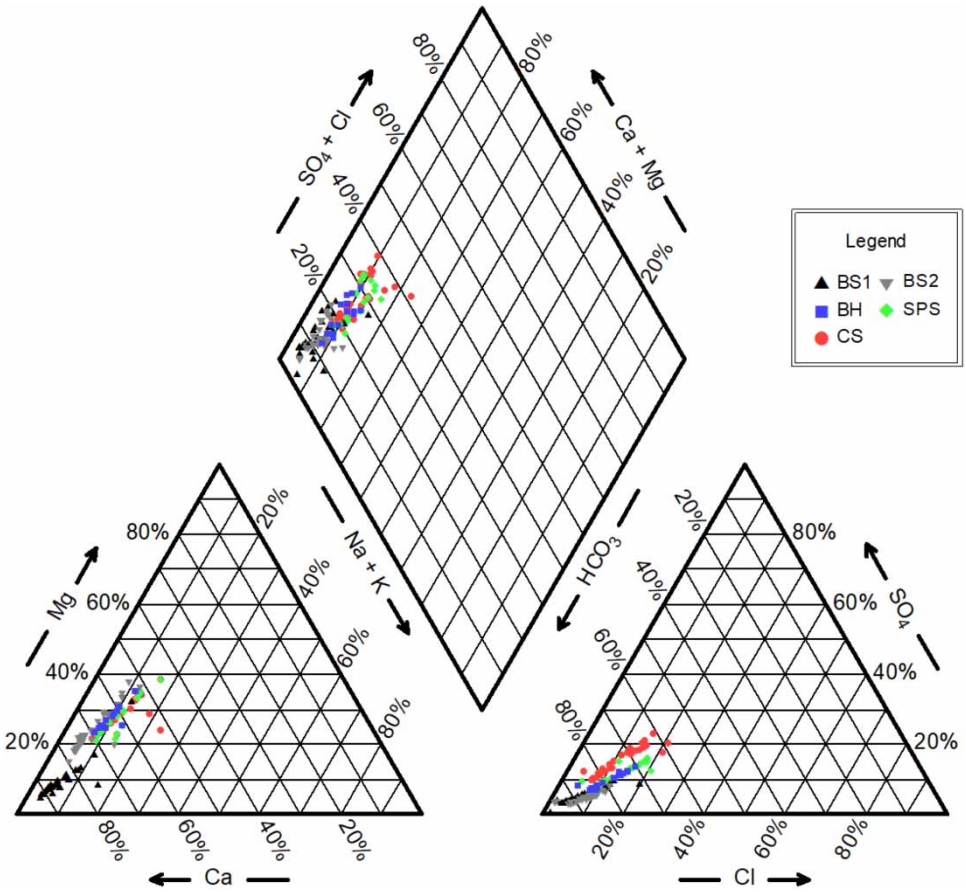

Figure 6 | Piper diagram of the hydrochemical dataset for the five springs.

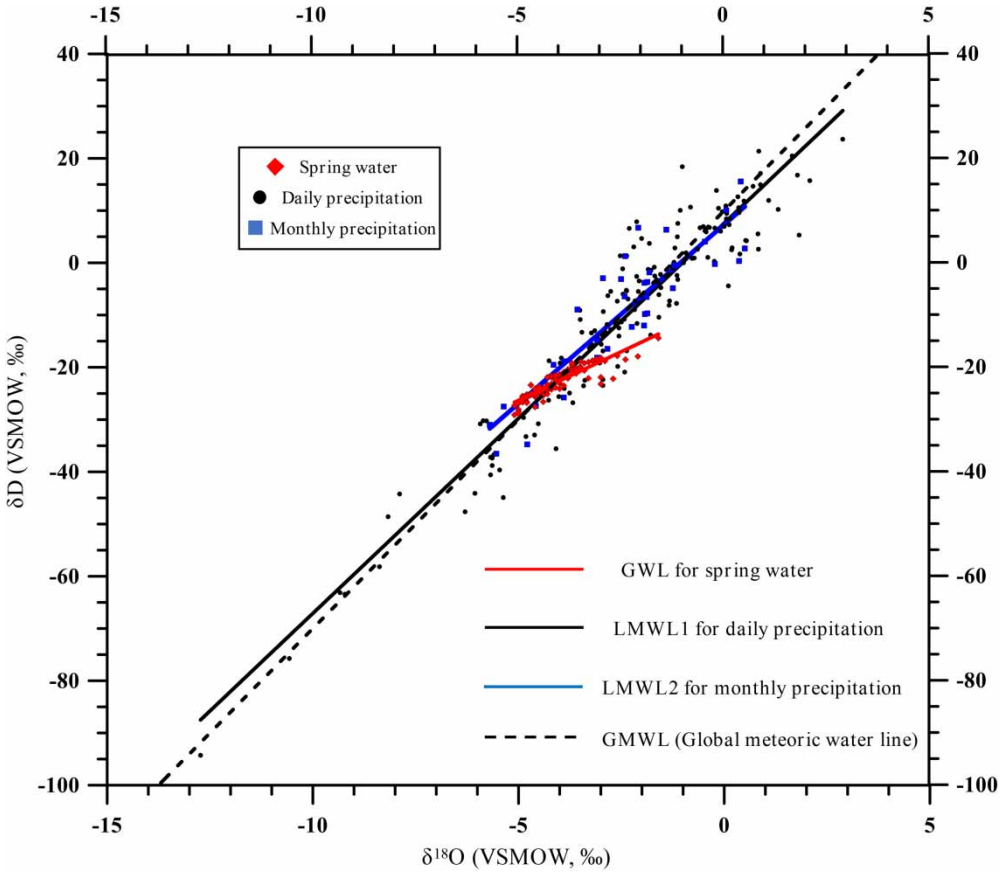

Figure 7 | Correlations between $\delta^{18}O$ and δD for the spring water (GWL) and their relations with the local meteoric water lines (LMWLs) and GMWL. The LMWLs are plotted using the isotopic data of daily precipitation (LMWL1) and monthly precipitation (LMWL2).

for the spring water is provided in Supplementary Material, Figure S4. The local meteoric water lines (LMWLs) are derived by the monthly and daily precipitation isotopic data using ordinary least squares regression (OLSR) (Crawford *et al.* 2014). The groundwater line (GWL) fits the data from the springs and plots below the LMWL, which are commonly interpreted as the characteristic of residual waters from partial evaporation (Bowen *et al.* 2018). The slope and intercept of LMWLs are close to each other; thus, monthly isotopic variability still preserves the isotopic signals of rain events. Most spring water samples fall close to the LMWL, indicating that the spring discharge undergoes minimal evaporation before precipitation recharge in general. A few spring water samples, especially from the three springs within the artesian zone, plot to the right of the LMWL with a decreased slope, which indicates a certain extent of evaporation for these samples. All the spring water are located on the lower part of the monthly precipitation, which suggests that the groundwater from the EA generally has relatively lighter isotopic signatures than the precipitation signals during 2017–2019.

The linear regression equations of LMWL1, LMWL2, and GWL are Equations (7)–(9), respectively. The uncertainties for slope and intercept of the water lines are provided with standard errors.

$$\text{LMWL1:}\delta D = (7.47 \pm 0.19)\,\delta^{18}O + (7.61 \pm 0.64) \quad (N = 157,\ R^2 = 0.91) \tag{7}$$

$$\text{LMWL2:}\delta D = (6.85 \pm 0.62)\,\delta^{18}O + (7.34 \pm 1.81) \quad (N = 34,\ R^2 = 0.79) \tag{8}$$

$$\text{GWL:}\delta D = (3.73 \pm 0.14)\,\delta^{18}O - (7.69 \pm 0.61) \quad (N = 148,\ R^2 = 0.82) \tag{9}$$

The global meteoric water line (GMWL) is defined as $\delta D = 8\delta^{18}O + 10$ (Craig 1961). The slopes and intercepts of LMWLs are slightly lower than the GMWL, which are controlled by local climatic factors. The intersection points between LMWLs and GWL are more negative compared with the amount weighted mean $\delta^{18}O$ (−2.7‰) in precipitation during 2017–2019. Long-term mean $\delta^{18}O$ in precipitation (from 1950 to present) in the study area is obtained from the Online Isotopes in Precipitation Calculator (OIPC, http://www.waterisotopes.org). The modeled long-term mean $\delta^{18}O$ in precipitation (−4.3‰) is close to the intersected $\delta^{18}O$ values between LMWLs and GWL, which indicates the theoretical initial spring recharge originated from the deep groundwater with longer residence time.

Violin plots of the isotopic variations for the springs and precipitation are shown in Figure 8. Tukey multiple comparisons for the means of isotopic signatures in the spring water and precipitation are provided in Supplementary

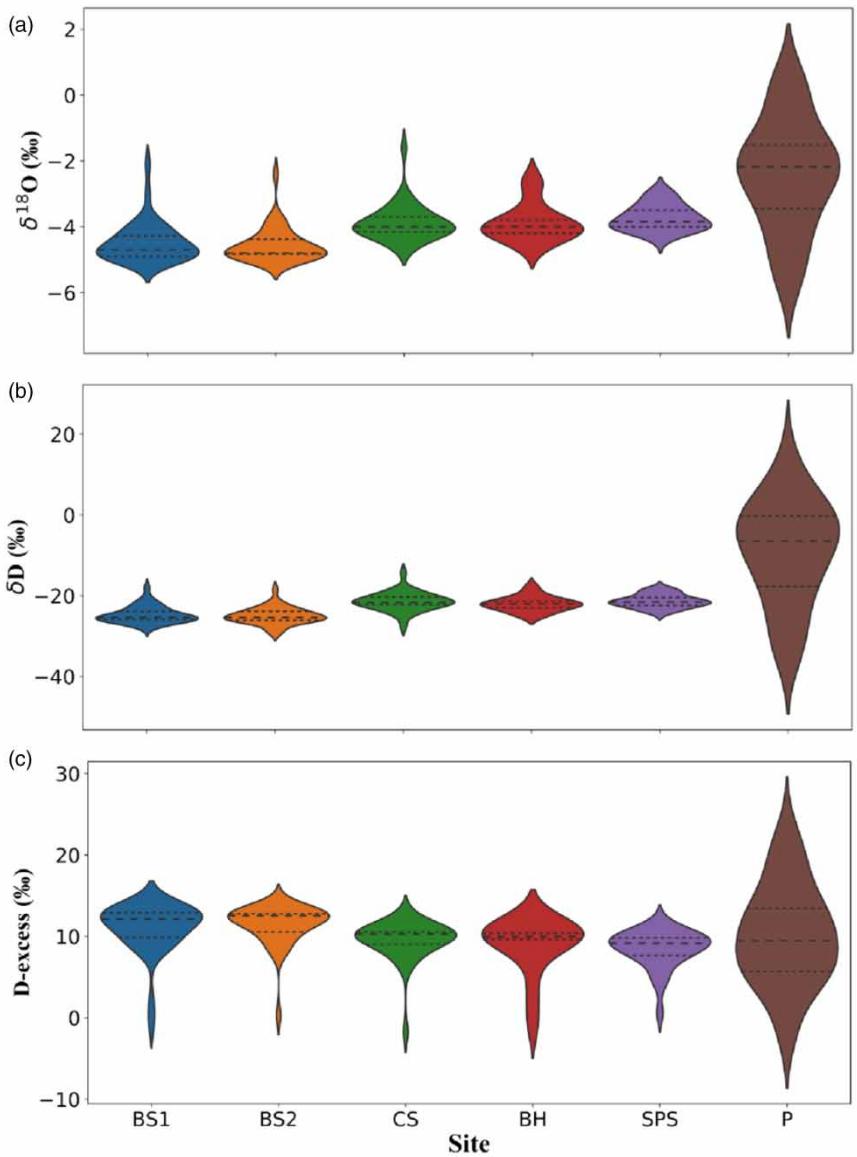

Figure 8 | Violin plots of the monthly $\delta^{18}O$ (a), δD (b), and D-excess (c) in the spring water and precipitation. The violin plots display the frequency (width of density plot), median (dashed line), and interquartile range (dotted line).

Material, Figure S5. There is no significant difference for $\delta^{18}O$ and δD among the three springs in the artesian zone (around −4.0‰ for $\delta^{18}O$), whereas two springs in the contributing zone have lighter isotopic signatures (around −4.5‰ for $\delta^{18}O$). The $\delta^{18}O$ and δD signals in precipitation have generally heavier isotopic signatures than the spring water. Thus, the springs from the contributing zone and artesian zone might have different contributions of deep and shallow groundwater. A few outliers above the $\delta^{18}O$ range for the springs might be the response to precipitation input or epikarst interflow. There is no significant difference for D-excess between the springs and precipitation (around 10‰). D-excess has been widely used to identify source regions of precipitation (e.g. Cui *et al.* 2009; Lewis *et al.* 2013; Steen-Larsen *et al.* 2015). However, D-excess might not be a good tracer for the springs in the mass balance calculations due to its significant variations. Thus, $\delta^{18}O$ of these springs is utilized to examine the possible precipitation input for the spring water balance later.

The temporal variations of $\delta^{18}O$ for the spring water and precipitation, together with the observed monthly precipitation amount in San Antonio, are shown in Figure 9. The amount weighted mean $\delta^{18}O$ of precipitation for all rain events during 2017–2019 is −2.7‰. The $\delta^{18}O$ of spring water shows small variations and varies below the mean $\delta^{18}O$ of precipitation during most of the time during 2017–2019. This demonstrates the bi-modal distribution of groundwater age for these three springs: the springs mainly originate from deep groundwater, with additional supplemental inputs from epikarst interflow or shallow groundwater.

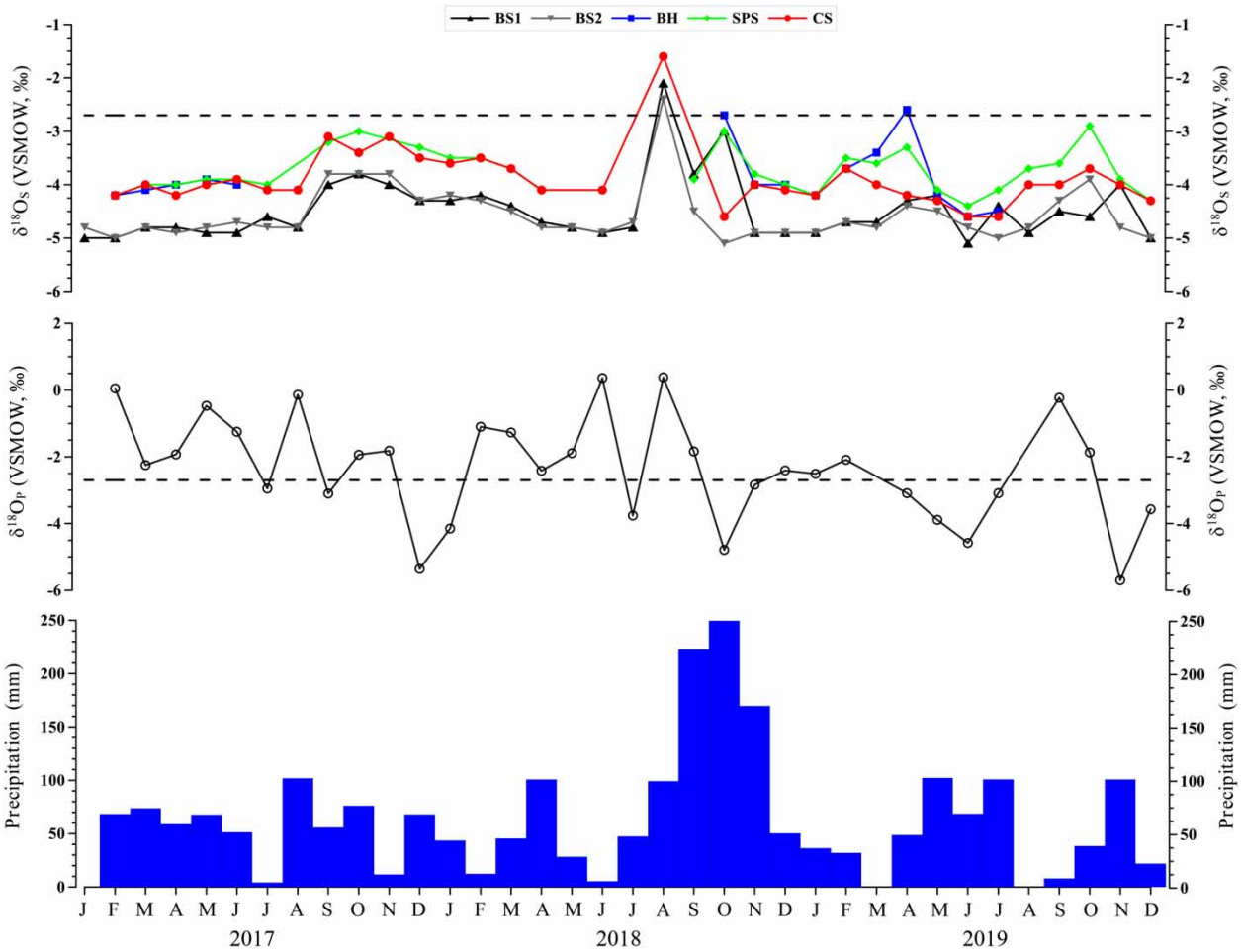

Figure 9 | Temporal variations of $\delta^{18}O$ for the five springs, $\delta^{18}O$ in precipitation, and precipitation amount during 2017–2019. The black dashed lines represent the amount weighted mean $\delta^{18}O$ for all rain events during 2017–2019.

The modeled long-term mean $\delta^{18}O$ in precipitation (from 1950 to present) is −4.3‰, and a weighted average $\delta^{18}O$ of −4.1‰ in precipitation (1999–2007) was obtained in a nearby city Austin, Texas (Pape *et al.* 2010). The springs investigated in this work display $\delta^{18}O$ signatures close to long-term mean $\delta^{18}O$ in precipitation, which indicates that these springs mainly originated from the deep groundwater with longer residence time. However, the amount weighted mean $\delta^{18}O$ for all rain events during 2017–2019 is −2.7‰, which is significantly higher than the mean $\delta^{18}O$ values observed in our spring sites and previously observed $\delta^{18}O$ in precipitation from Texas. The enriched $\delta^{18}O$ values in precipitation during 2017–2019 might be due to higher annual mean temperatures or increasing seasonal variability of precipitation.

The isotopic signatures for the five investigated springs demonstrate similar trends; however, the springs in the contributing zone (BS1 and BS2) generally have lighter isotopic signatures than the springs in the artesian zone (CS, BH, and SPS). The isotopic signatures of precipitation have higher variations than the spring water. There is no lag or 1-month lag of this response for $\delta^{18}O$ in springs to $\delta^{18}O$ in precipitation. Thus, there is additional 'young' precipitation input for springs beside the 'old' deep groundwater, and this 'young' shallow groundwater could reach these spring sites within 1 month. The response of $\delta^{18}O$ in springs to precipitation input is also related to the precipitation amount. For example, June and August 2018 have the heaviest isotopic signals, but there is no response of isotopic signals in June 2018 due to its small precipitation amount. The precipitation input is likely from the epikarst interflow, which agrees with its quick response and short-lasting time.

Mass balance calculations

Since all springs have consistent isotopic signals (also the lowest $\delta^{18}O$ values) during their base flow conditions (Figure 9), we directly use the lightest isotopic values for the investigated springs as their endmember of $\delta^{18}O_{DG}$ for deep groundwater: −5.1‰ (BS1 and BS2); −4.6‰ (BH and CS); −4.4‰ (SPS). Since most spring water undergoes minimal evaporation before precipitation recharge (Figure 7), and 'young' shallow groundwater could reach these spring sites within 1 month (Figure 3), $\delta^{18}O^{N}_{SG}$ for shallow groundwater could be directly assigned as $\delta^{18}O$ in precipitation for each monthly interval calculated by Equation (4). Our observed isotopic data of daily precipitation are consistent with those observed in a previous event-based isotopic study of precipitation during 2015–2017 in Austin (Sun *et al.* 2019). We assumed that $\delta^{18}O$ in precipitation might be spatiotemporally homogeneous in Central Texas and assigned the same $\delta^{18}O_{SG}$ for the investigated springs. In that sense, the altitude effect on the isotope in precipitation is considered limited in the research area. The altitude of the rain collector is 303 m, about 170 m lower than the two springs (BS1 and BS2) from the unconfined zone and 100 m higher than the three springs (BH, SPS, and CS) from the confined zone. However, the altitudinal lapse rate is unknown in the study area, which is the primary source of uncertainty in our isotope mixing model.

The monthly F_{SG} results for the five springs are shown in Figure 10(a). Note that the isotope mixing model would not return F_{DG} and F_{SG} contribution estimates when the isotopic values for spring water and the endmembers have no significant differences. The amount weighted mean $\delta^{18}O$ in precipitation during 2017–2019 is −2.7‰, which could be utilized as the endmember of mean $\delta^{18}O_{SG}$ during 2017–2019, assuming that all precipitation events lead to recharge. The overall F_{DG} and F_{SG} results for the five spring during 2017–2019 are shown in Figure 10(b). The monthly F_{SG} for all springs display broad ranges of change from 0 to 80%. The monthly F_{SG} for the five springs demonstrate similar trends during 2017–2019, which verified the isotope mixing model's validity. The overall F_{SG} during 2017–2019 varied from 20 to 40% (an average of 33%); however, the three springs in the artesian zone (an average of 39%) have higher overall F_{SG} than the two springs in the contributing zone (an average of 25%). The relatively high contributions of precipitation input for spring in the artesian zone might be due to their relatively lower elevation and larger catchment area than the springs in the contributing zone. This elevated input from epikarst interflow for springs within the artesian zone agrees with the evolved hydrochemical types from HCO_3–Ca type to HCO_3·Cl–Ca·Mg type from the contributing zone to the artesian zone, which verified the validity of the isotope mixing model.

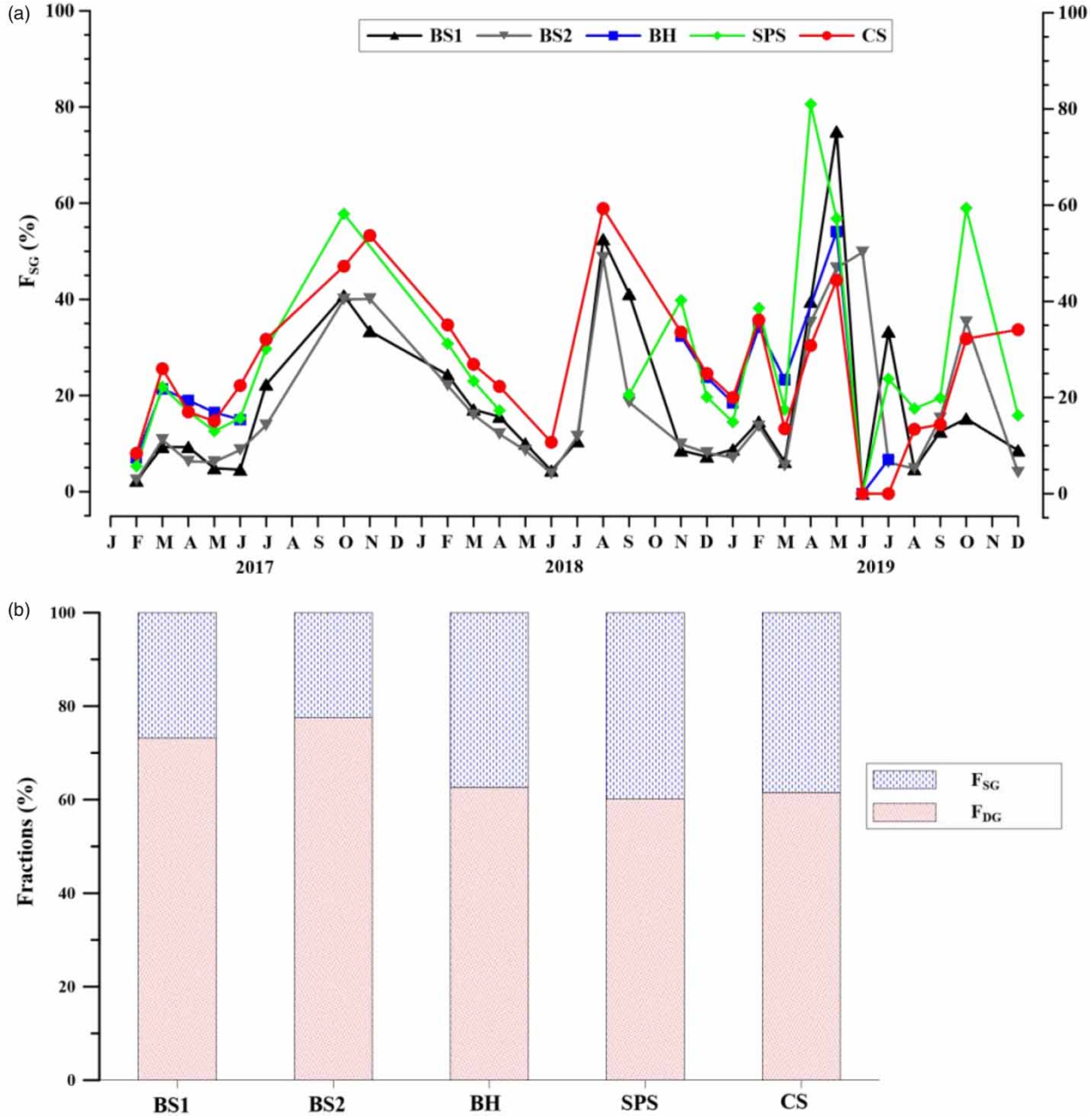

Figure 10 | Water balance calculation results of monthly F_{SG} (a) and overall F_{DG}/F_{SG} during 2017–2019 (b) for the five springs.

CONCLUSIONS

This research has investigated isotopic signatures of five springs from the EA region, two springs from the unconfined section and three from the confined section, by monthly sampling during 2017–2019. There is a quick response for isotopic signals in spring water to changes in the isotopic compositions of precipitation. By utilizing the isotope mixing model, we have identified sources of water for these springs with a bi-modal distribution of groundwater age: mainly originate from deep groundwater (an average of 67%), with additional supplement shallow groundwater (an average of 33%). With the evolved hydrochemical type from HCO_3–Ca type to HCO_3·Cl–Ca·Mg type along the EA

flowpaths, there is elevated input from epikarst interflow for spring water balance in the artesian zone than the contributing zone.

There is a lack of quantitative analysis on ages of the spring water due to no proper dating methods. Our isotope mixing model could untangle groundwater mixing ratios (shallow vs. deep groundwater) and travel times (short vs. long residence time) within the EA. However, there are several caveats in our isotope mixing models: the altitude effect on the isotope in precipitation is considered limited in the research area; we assume that spring water generally undergoes minimal evaporation; the monthly sampling of spring water may not be representative of temporal isotopic variations. More systematical investigations on the evolution of isotopic signatures from precipitation to groundwater are needed to refine the isotope mixing model in future research.

ACKNOWLEDGEMENTS

We thank Stuart Brown, Gary Rogers, Erica Martinez and Yuanxin Qu for their assistance with property access and water sampling. Gabrielle Timmins and Ashley Cottrell are thanked for their contributions to analyzing dissolved ions in the Texas State University Laboratory. The authors thank Dr Przemyslaw Wachniew (Associate Editor) and two anonymous reviewers for their valuable comments and suggestions. The activities reported here were funded in part by the Edwards Aquifer Authority (EAA) under Interlocal Cooperation Contract No. 19-928-AMS, but this work does not necessarily reflect the view or regulatory position of the EAA. This research was also funded in part by the National Key Research and Development Program of China (2016YFA0600504 and 2020YFA0607700), the Strategic Priority Research Program of the Chinese Academy of Sciences (XDB26000000), and the National Natural Science Foundation of China (41888101 and 41690114).

DATA AVAILABILITY STATEMENT

All relevant data are included in the paper or its Supplementary Information.

REFERENCES

Araguás-Araguás, L., Froehlich, K. & Rozanski, K. 2000 Deuterium and oxygen-18 isotope composition of precipitation and atmospheric moisture. *Hydrological Processes* **14** (8), 1341–1355. https://doi.org/10.1002/1099-1085(20000615)14:8 < 1341::AID-HYP983 > 3.0.CO;2-Z.

Bowen, G. J., Putman, A., Brooks, J. R., Bowling, D. R., Oerter, E. J. & Good, S. P. 2018 Inferring the source of evaporated waters using stable H and O isotopes. *Oecologia* **187** (4), 1025–1039. https://doi.org/10.1007/s00442-018-4192-5.

Chaudhuri, S. & Ale, S. 2014 Temporal evolution of depth-stratified groundwater salinity in municipal wells in the major aquifers in Texas, USA. *Science of the Total Environment* **472**, 370–380. https://doi.org/10.1016/j.scitotenv.2013.10.120.

Chen, X., Zhang, Y. F., Xue, X., Zhang, Z. & Wei, L. 2012 Estimation of baseflow recession constants and effective hydraulic parameters in the karst basins of southwest China. *Hydrology Research* **43** (1–2), 102–112. https://doi.org/10.2166/nh.2011.136.

Cox, W. D., Meng, L., Khedun, C. P., Nordfelt, A. & Quiring, S. M. 2009 Discharge variability for an artesian spring of the Edwards Aquifer: Comal Springs (1933–2007). *International Journal of Climatology* **29** (15), 2324–2336. https://doi.org/10.1002/joc.1871.

Craig, H. 1961 Standard for reporting concentrations of deuterium and oxygen-18 in natural waters. *Science* **133** (3467), 1833–1834. https://doi.org/10.1126/science.133.3467.1833.

Crawford, J., Hughes, C. E. & Lykoudis, S. 2014 Alternative least squares methods for determining the meteoric water line, demonstrated using GNIP data. *Journal of Hydrology* **519**, 2331–2340. https://doi.org/10.1016/j.jhydrol.2014.10.033.

Cui, J., An, S., Wang, Z., Fang, C., Liu, Y., Yang, H., Zhen, X. & Liu, S. 2009 Using deuterium excess to determine the sources of high-altitude precipitation: implications in hydrological relations between sub-alpine forests and alpine meadows. *Journal of Hydrology* **373** (1–2), 24–33. https://doi.org/10.1109/ISWREP.2011.5893678.

Dansgaard, W. 1964 Stable isotopes in precipitation. *Tellus* **16** (4), 436–468. https://doi.org/10.3402/tellusa.v16i4.8993.

Eberts, S., Martha, L. J., MaryLynn, M., Richard, J. L. & Lynne, F. 2011 Assessing the Vulnerability of Public-Supply Wells to Contamination: Edwards Aquifer Near San Antonio, Texas. USGS Fact Sheet.

Engesgaard, P. & Christensen, T. H. 1988 A review of chemical solute transport models. *Hydrology Research* **19** (3), 183–216. https://doi.org/10.2166/nh.1988.0013.

Gröning, M., Lutz, H. O., Roller-Lutz, Z., Kralik, M., Gourcy, L. & Pöltenstein, L. 2012 A simple rain collector preventing water re-evaporation dedicated for $\delta^{18}O$ and $\delta^{2}H$ analysis of cumulative precipitation samples. *Journal of Hydrology* **448**, 195–200. https://doi.org/10.1016/j.jhydrol.2012.04.041.

Halihan, T. & Wicks, C. M. 1998 Modeling of storm responses in conduit flow aquifers with reservoirs. *Journal of Hydrology*

208 (1–2), 82–91. https://doi.org/10.1016/S0022-1694(98)00149-8.

Hare, D. K., Helton, A. M., Johnson, Z. C., Lane, J. W. & Briggs, M. A. 2021 Continental-scale analysis of shallow and deep groundwater contributions to streams. *Nature Communications* **12** (1), 1–10. https://doi.org/10.1038/s41467-021-21651-0.

Hovorka, S. D., Mace, R. E. & Collins, E. W. 1995 Regional distribution of permeability in the Edwards Aquifer. *GCAGS Transactions* **45**, 259–265.

Hunt, B., Smith, B. A., Campbell, S., Beery, J., Hauwert, N. & Johns, D. 2005 Dye tracing recharge features under high-flow conditions, Onion Creek, Barton Springs Segment of the Edwards Aquifer, Hays County, Texas. *Austin Geological Society Bulletin* **1**, 70–86.

Hunt, A. G., Landis, G. P. & Faith, J. R. 2016 *Groundwater Ages from the Freshwater Zone of the Edwards Aquifer, Uvalde County, Texas – Insights Into Groundwater Flow and Recharge*. US Geological Survey, No. 2015-5163.

Hunt, B. B., Smith, B. A. & Hauwert, N. M. 2019 Barton Springs segment of the Edwards (Balcones Fault Zone) Aquifer, Central Texas. In: *The Edwards Aquifer: The Past, Present, and Future of a Vital Water Resource* (J. M. Sharp, R. T. Green Jr. & G. M. Schindel, eds). Geological Society of America Memoir 215, pp. 75–100. https://doi.org/10.1130/2019.1215(07).

Jiang, Y., Zhang, C., Yuan, D., Zhang, G. & He, R. 2008 Impact of land use change on groundwater quality in a typical karst watershed of southwest China: a case study of the Xiaojiang watershed, Yunnan Province. *Hydrogeology Journal* **16** (4), 727–735. https://doi.org/10.1007/s10040-007-0259-9.

Klemt, W. B., Knowles, T. R., Elder, G. R. & Sieh, T. W. 1979 *Ground-Water Resources and Model Applications for the Edwards (Balcones Fault Zone) Aquifer in the San Antonio Region, Texas*. Department of Water Resources Report No. 239, Texas.

Kuniansky, E. L., Fahlquist, L. & Ardis, A. F. 2001 Travel times along selected flow paths of the Edwards Aquifer, central Texas. In: *U.S. Geological Survey Karst Interest Group Proceedings* (E. L. Kuniansky, ed.). Water-Resources Investigations Report 01-4011, pp. 69–77.

Lewis, S. C., LeGrande, A. N., Kelley, M. & Schmidt, G. A. 2013 Modeling insights into deuterium excess as an indicator of water vapor source conditions. *Journal of Geophysical Research: Atmospheres* **118** (2), 243–262. https://doi.org/10.1029/2012JD017804.

Maloszewski, P. & Zuber, A. 1991 Influence of matrix diffusion and exchange reactions on radiocarbon ages in fissured carbonate aquifers. *Water Resources Research* **27** (8), 1937–1945. https://doi.org/10.1029/91WR01110.

Marfia, A. M., Krishnamurthy, R. V., Atekwana, E. A. & Panton, W. F. 2004 Isotopic and geochemical evolution of ground and surface waters in a karst dominated geological setting: a case study from Belize, Central America. *Applied Geochemistry* **19** (6), 937–946. https://doi.org/10.1016/j.apgeochem.2003.10.013.

Martinez, J. L., Raiber, M. & Cox, M. E. 2015 Assessment of groundwater–surface water interaction using long-term hydrochemical data and isotope hydrology: headwaters of the Condamine River, Southeast Queensland, Australia. *Science of the Total Environment* **536**, 499–516. https://doi.org/10.1016/j.scitotenv.2015.07.031.

Michelsen, N., van Geldern, R., Roßmann, Y., Bauer, I., Schulz, S., Barth, J. A. & Schüth, C. 2018 Comparison of precipitation collectors used in isotope hydrology. *Chemical Geology* **488**, 171–179. https://doi.org/10.1016/j.chemgeo.2018.04.032.

Moore, P. J., Martin, J. B. & Screaton, E. J. 2009 Geochemical and statistical evidence of recharge, mixing, and controls on spring discharge in an eogenetic karst aquifer. *Journal of Hydrology* **376** (3–4), 443–455. https://doi.org/10.1016/j.jhydrol.2009.07.052.

Morrall, D., McAvoy, D., Schatowitz, B., Inauen, J., Jacob, M., Hauk, A. & Eckhoff, W. 2004 A field study of triclosan loss rates in river water (Cibolo Creek, TX). *Chemosphere* **54** (5), 653–660. https://doi.org/10.1016/j.chemosphere.2003.08.002.

Pape, J. R., Banner, J. L., Mack, L. E., Musgrove, M. & Guilfoyle, A. 2010 Controls on oxygen isotope variability in precipitation and cave drip waters, Central Texas, USA. *Journal of Hydrology* **385** (1–4), 203–215. https://doi.org/10.1016/j.jhydrol.2010.02.021.

Retike, I., Kalvans, A., Popovs, K., Bikse, J., Babre, A. & Delina, A. 2016 Geochemical classification of groundwater using multivariate statistical analysis in Latvia. *Hydrology Research* **47** (4), 799–813. https://doi.org/10.2166/nh.2016.020.

Schindel, G. M. 2019 Genesis of the Edwards (Balcones Fault Zone) Aquifer. In: *The Edwards Aquifer: The Past, Present, and Future of a Vital Water Resource* (J. M. Sharp, R. T. Green Jr. & G. M. Schindel, eds). Geological Society of America Memoir 215, pp. 9–18. https://doi.org/10.1130/2019.1215(02).

Schindel, G. M., Hoyt, J. R. & Johnson, S. B. 2004 The Edwards Aquifer of south-central Texas, USA. In: *Encyclopedia of Cave and Karst Sciences* (J. Gunn, ed.). Fitzroy Dearborn Publishers, London, pp. 313–315.

Shakya, B. M., Nakamura, T., Shrestha, S. D. & Nishida, K. 2019 Identifying the deep groundwater recharge processes in an intermountain basin using the hydrogeochemical and water isotope characteristics. *Hydrology Research* **50** (5), 1216–1229. https://doi.org/10.2166/nh.2019.164.

Sharp Jr., J. M. & Banner, J. L. 1997 The Edwards Aquifer: a resource in conflict. *GSA Today* **7** (8), 1–9.

Steen-Larsen, H. C., Sveinbjörnsdottir, A. E., Jonsson, T., Ritter, F., Bonne, J. L., Masson-Delmotte, V., Sodemann, H., Blunier, T., Dahl-Jensen, D. & Vinther, B. M. 2015 Moisture sources and synoptic to seasonal variability of North Atlantic water vapor isotopic composition. *Journal of Geophysical Research: Atmospheres* **120** (12), 5757–5774. https://doi.org/10.1002/2015JD023234.

Stone, D. & Schindel, G. M. 2002 The application of GIS in support of land acquisition for the protection of sensitive groundwater recharge properties in the Edwards Aquifer of

south-central Texas. *Journal of Cave and Karst Studies* **64** (1), 38–44.

Sullivan, T. P. & Gao, Y. 2016 Assessment of nitrogen inputs and yields in the Cibolo and Dry Comal Creek watersheds using the SWAT model, Texas, USA 1996–2010. *Environmental Earth Sciences* **75** (9), 725. https://doi.org/10.1007/s12665-016-5546-0.

Sullivan, T. P., Gao, Y. & Reimann, T. 2019 Nitrate transport in a karst aquifer: numerical model development and source evaluation. *Journal of Hydrology* **573**, 432–448. https://doi.org/10.1016/j.jhydrol.2019.03.078.

Sun, C., Shanahan, T. M. & Partin, J. 2019 Controls on the isotopic composition of precipitation in the south-central United States. *Journal of Geophysical Research: Atmospheres* **124** (14), 8320–8335. https://doi.org/10.1029/2018JD029306.

Tian, L., Smith, B., Hunt, B., Doster, J. D. & Gao, Y. 2020 Geochemical evaluation of hydrogeologic interaction between the Edwards and Trinity Aquifers based on multiport well assessment in Central Texas. In: *Proceedings of the 16th Multidisciplinary Conference on Sinkholes and the Engineering and Environmental Impacts of Karst* (L. Land, C. Kromhou & M. J. Byle, eds). National Cave and Karst Research Institute Symposium 8, pp. 269–277. https://doi.org/10.5038/9781733375313.1032.

Wang, Y., Song, X., Li, B., Ma, Y., Zhang, Y., Yang, L., Bu, H. & Holm, P. E. 2018 Temporal variation in groundwater hydrochemistry driven by natural and anthropogenic processes at a reclaimed water irrigation region. *Hydrology Research* **49** (5), 1652–1668. https://doi.org/10.2166/nh.2018.123.

Zhang, A., Winterle, J. & Yang, C. 2020 Performance comparison of physical process-based and data-driven models: a case study on the Edwards Aquifer, USA. *Hydrogeology Journal* **28** (6), 2025–2037. https://doi.org/10.1007/s10040-020-02169-z.

First received 18 January 2021; accepted in revised form 5 May 2021. Available online 20 May 2021